

See discussions, stats, and author profiles for this publication at: <https://www.researchgate.net/publication/265793791>

# Cadmium Vacancy Minority Defects as Luminescence Centers in Size and Strain Dependent Photoluminescence Shifts in CdS Nanotubes

ARTICLE *in* THE JOURNAL OF PHYSICAL CHEMISTRY C · AUGUST 2014

Impact Factor: 4.77 · DOI: 10.1021/jp503954y

---

CITATIONS

3

READS

50

## 3 AUTHORS, INCLUDING:



**Prasenjit Ghosh**

Indian Institute of Science Education and Res...

25 PUBLICATIONS 210 CITATIONS

[SEE PROFILE](#)



**Shouvik Datta**

Indian Institute of Science Education and Res...

34 PUBLICATIONS 182 CITATIONS

[SEE PROFILE](#)

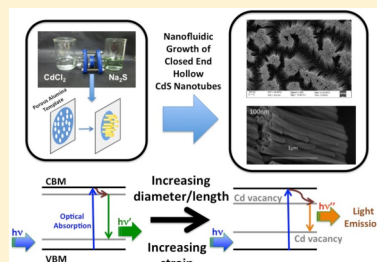
# Cadmium Vacancy Minority Defects as Luminescence Centers in Size and Strain Dependent Photoluminescence Shifts in CdS Nanotubes

Arthur Varghese,<sup>†</sup> Prasenjit Ghosh,<sup>\*,†,‡</sup> and Shouvik Datta<sup>\*,†</sup>

<sup>†</sup>Department of Physics and <sup>‡</sup>Department of Chemistry, Indian Institute of Science Education and Research, Pune 411008, India

 Supporting Information

**ABSTRACT:** We have studied the absorbance and photoluminescence properties of cadmium sulfide nanotubes with overall size beyond the quantum confinement regime. While the absorption spectra are unaffected by the change in size there is an anomalous red-shift in the photoluminescence spectra with increase in size. Using density functional calculations, we have identified that the shift in the emission peak of the photoluminescence spectra is a result of the interplay between Cd vacancies on the surface of these nanotubes and the crystalline strain which was incorporated in these nanotubes during their growth process. Most importantly, our results show that rather than the defect concentration, it is the nature of the defect which plays a crucial role in determining the optical properties of these nanotubes. For this particular case of CdS nanotubes we find that though S interstitials are the most abundant ones, however, it is the Cd vacancies with second lowest formation energies which significantly affect the photoluminescence spectra.



## 1. INTRODUCTION

Semiconductor nanostructures of metal oxides and chalcogenides have attracted immense attention due to their interesting size tunable physical properties arising from quantum confinement.<sup>1–4</sup> They offer a rich playground for fundamental science as well as for optoelectronic applications like solar cells,<sup>5</sup> lasers,<sup>6</sup> field effect transistors, field effect emitters,<sup>7,8</sup> etc. Optical properties of these nanostructured materials, which give rise to the above-mentioned applications, are influenced by several factors, namely, (i) their small size due to which they exhibit quantum confinement effects, (ii) the nature and the concentration of the defects formed during their synthesis, and (iii) the strain induced in these materials during the growth/nucleation process. While the quantum confinement effects are predominant in the nanostructures whose sizes are comparable to the Bohr exciton radius, the other factors affect the optical properties of these nanostructures irrespective of their size. There have been efforts to understand the role of the above-mentioned factors on the optical properties of the nanostructures of both the metal chalcogenides and oxides. For example, Kim et al. showed that high defect concentration in CdS quantum dots using low temperature synthesis methods leads to only 1% photoluminescence quantum efficiency.<sup>9</sup> Moreover, the luminescent mechanisms of quantum dots could be different based on different synthetic routes.<sup>10,11</sup> There have been efforts to engineer the band gap of CdS nanowires<sup>12</sup> and ZnO microwires<sup>13</sup> by applying an external strain field. Recently an anomalous luminescence blue-shift has been observed in ZnO nanorods<sup>14</sup> and CdSe nanowires<sup>15</sup> with sizes beyond the quantum confinement regime. However, most of these anomalous shifts were attributed to surface effects due to increased surface to volume ratio for the case of ZnO and the band filling effect due to Se vacancies for CdSe.

Here we investigate similar luminescence shifts in hollow nanotubes of cadmium sulfide (CdS) with respect to their length and diameters. Cadmium sulfide (CdS), a II–VI semiconductor, with bulk band gap of about 2.42 eV is an important material which has been of immense interest to scientists recently.<sup>16</sup> CdS can simultaneously act as a light harvester and carrier transporter. Moreover, CdS nanotubes form a direct and rapid transport channel for photogenerated electrons because the electron mobility in CdS material ( $210 \text{ cm}^2 (\text{V s})^{-1}$ ) is much higher than that in TiO<sub>2</sub> and ZnO. Additionally, the tubular structure has a large surface area which results in efficient hole transportation when they are in contact with an electrolyte, thereby reducing electron–hole recombination.<sup>17,18</sup> All these properties make CdS nanotubes a plausible candidate for semiconductor sensitized solar cells (SSSC)<sup>19,20</sup> and photocatalyst for photocatalytic splitting of water.<sup>21–23</sup> However, the properties of these nanotubes depend on how they are synthesized since the nature and defect concentrations and the inbuilt strain in these nanotubes are sensitive toward the synthesis method. Therefore, for possible use of the nanotubes, it is important to have a proper understanding of the effect of quantum confinement, defects, and strain on the optical properties of nanotubes. However, most of the reported studies of the optical properties of the CdS nanostructures are focused on the quantum dots (QD). To the best of our knowledge, there are very few systematic studies of the role of defects on the electronic properties of one-dimensional CdS nanostructures.<sup>24</sup> However, we would like to point out that the nature of defects in zero dimensional

**Received:** April 23, 2014

**Revised:** August 26, 2014

**Published:** August 26, 2014



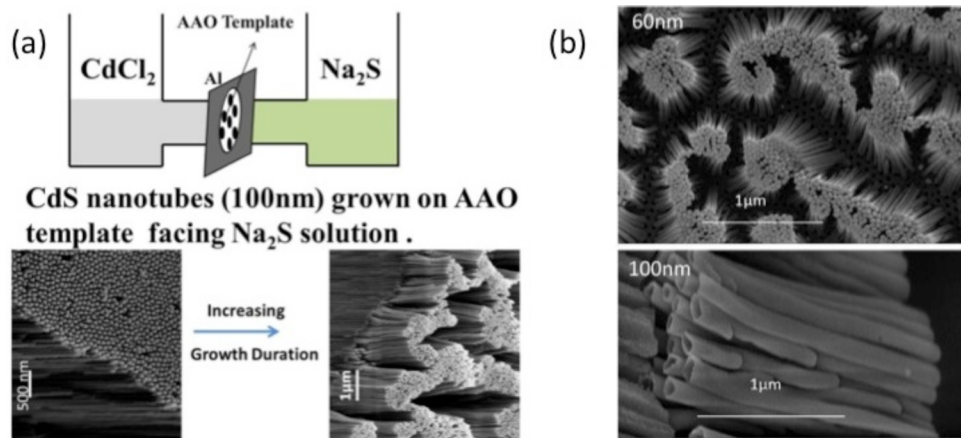


**Figure 1.** (a) Schematic picture of the setup used for synthesis of CdS nanotubes attached with porous alumina (AAO) template. Scanning electron microscopy (SEM) images clearly show that length of these nanotube are increasing with increasing growth duration. (b) SEM images of CdS nanotubes having diameters of about 60 and 100 nm. It is clear that nanotubes are forming at the edge of porous alumina nanochannels.

QDs are different from those of the one-dimensional nanotubes or nanowires. While for the former the defects are primarily uncompensated dangling bonds or charged surface states, etc., for the latter the majority of the defects are stoichiometric defects rising from vacancies, interstitials, or anti sites.<sup>25</sup> Hence, there is a need for systematic study of defects and the effect of strain on the energy positions of the defect states in the nanotubes to understand how strain and defects can affect their optical properties.

In this paper, with a combination of experiments and *ab initio* density functional theory, we have studied the absorption and photoluminescence (PL) properties of CdS nanotubes grown horizontally using free-standing nano porous alumina membrane (AAO)<sup>26</sup> as a function of their length and diameter. Diameters of these nanotubes are well beyond the quantum confinement regime of CdS having a Bohr exciton radius of about 3 nm—the smallest one having a diameter around 22 nm while the diameter of the largest one being 100 nm. Additionally, the thickness of the walls of the nanotubes is also of the order of 10–15 nm. This enables us to study exclusively the role of defects in these nanotubes, since we can expect that the quantum confinement effects are not significant in them. In addition to the probability of having defects, these nanotubes also experience inbuilt crystalline strain which was incorporated during sustained growth nucleation while they grow horizontally from one side of the alumina template. We have explored the role of defects and strain in order to rationalize the experimentally measured variations in absorption and PL spectra. We have tried to establish that the most abundant electronic defects need not be the most effective luminescence center. Our calculations clearly show that other “not-so-abundant” cadmium vacancy minority defects whose properties vary systematically with the size of these nanotube can in fact affect the luminescence spectra as a function of induced strain during the growth nucleation. The rest of the paper is organized as follows: in sections 2 and 3 we provide the experimental and computational details. The experimental results and first principles calculation results are presented in section 4. Finally, we discuss the implications of our results and summarize in section 5.

## 2. EXPERIMENTAL DETAILS

CdS nanotubes having different outer diameters and lengths were synthesized using porous alumina (AAO) nanochannels by a two-chamber method (Figure 1a) as reported in the past.<sup>26</sup> AAO templates having different nanochannels diameters are prepared by anodizing 99% pure aluminum foil at different anodization voltages (18, 25, 40, 50, and 60 V). To begin with, reactants in both chambers were physically separated by AAO template with (0.1 M)  $\text{CdCl}_2$  on one side and (0.1 M)  $\text{Na}_2\text{S}$  in deionized water on the other side. These reactants can flow through these nanochannels and physically mix and react to form CdS nanotubes only on  $\text{Na}_2\text{S}$  side of the AAO template.<sup>26</sup> After few hours of synthesis, the AAO template visibly changes color from transparent white to yellowish orange. Scanning electron microscopy images of as-prepared CdS nanotubes protruding out of these AAO template were recorded using Carl Zeiss Ultra Plus field emission scanning electron microscope (FESM) (Figure 1a,b). UV-vis optical absorption studies were done with a PerkinElmer Lambda950 UV-vis-IR spectrophotometer with scan steps of 1 nm, and the photoluminescence spectra of all solid samples were measured using a Horiba-JobinYvon FluoroLog-3 fluorescence spectrometer with scan steps of 1 nm and excited at 2.95 eV (420 nm). The crystalline nature of CdS nanotubes with different diameters was identified with Bruker Advance-D powder X-ray diffractometer with  $\text{Cu K}\alpha$  X-ray radiation (0.154 nm) and scan increment of 0.01° per step.

## 3. COMPUTATIONAL DETAILS

We have performed density functional theory (DFT) based calculation with plane-wave basis set as implemented in the Quantum ESPRESSO software.<sup>27</sup> The exchange-correlation potential is described by the generalized gradient approximation (GGA) based parametrization by Purdew, Burke, and Erzenhof (PBE).<sup>28</sup> Electron–ion interactions have been described by ultrasoft pseudopotentials.<sup>29</sup> We have used 40 and 400 Ry as kinetic energy cutoffs for wave function and charge density, respectively. For speeding up the convergence, we have used Marzari–Vanderbilt smearing of 0.001 Ry.<sup>30</sup>

For bulk CdS we have considered the wurtzite structure since in the experimental reports, the CdS nanotubes have similar structure. Our calculations yield the lattice parameter for bulk CdS to be 4.20 Å. We obtain the *c/a* ratio and internal

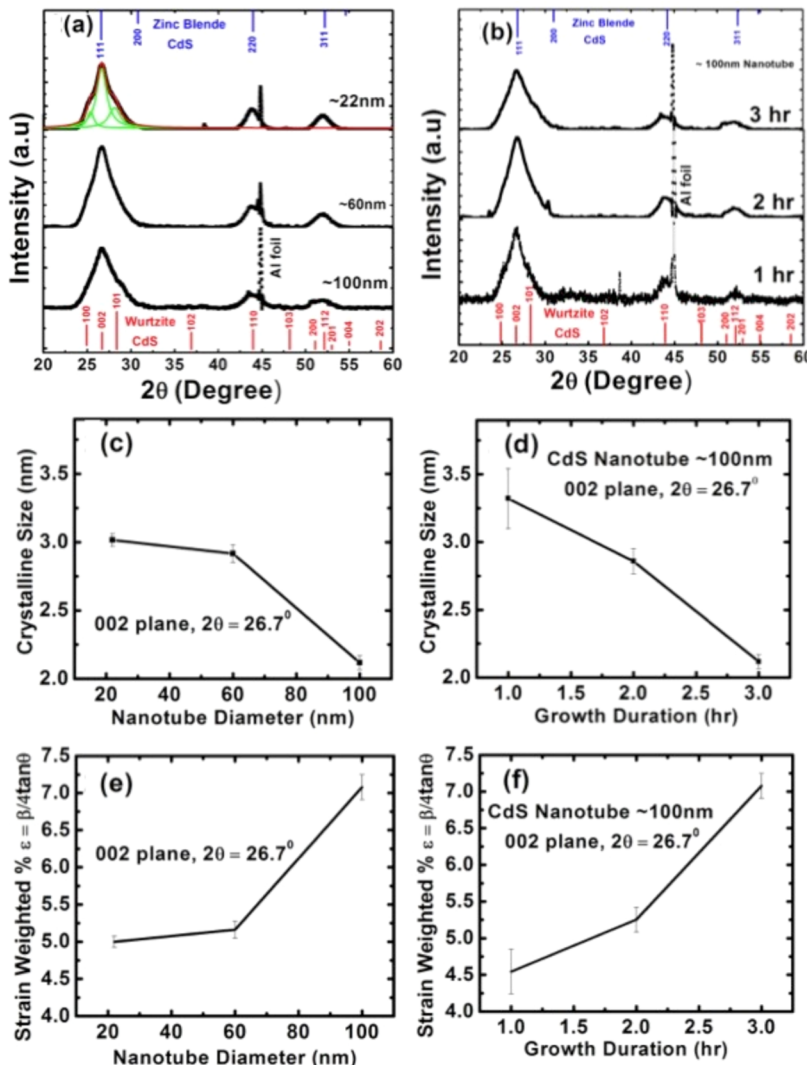


**Figure 2.** X-ray diffraction spectrum of CdS nanotubes having (a) different diameters and (b) different growth durations (or lengths) with outer diameter of about 100 nm. Sharp feature around  $2\theta$  of  $45^\circ$  is from the aluminum (Al) background only. For better clarity in presentation, in (a) we have indicated one such representative deconvolution of this composite XRD peak to estimate the integral breadth of the central (002) peak. (c) and (d) are calculated crystallite sizes as a function of their diameter and growth durations (lengths), respectively. (e) and (f) are the calculated weighted average % strain for CdS nanotubes having different diameters and growth durations (lengths), respectively.

parameter  $u$  to be 1.63 and 0.376, respectively. Our results are in excellent agreement with previous calculations<sup>31</sup> and experimental measurements.<sup>32,33</sup> The computed band gap for CdS is 1.12 eV, which is severely underestimated compared to the experimental band gap of 2.42 eV at room temperature.<sup>34</sup> This is a well-known shortcoming of DFT electronic structure calculations. However, we note that though the absolute values of band gaps obtained from a DFT calculation is severely underestimated, the qualitative trends are correctly predicted.

In order to study the effects of defects (neutral) and strain in the CdS nanotube, we considered a single shelled CdS nanotube containing six CdS molecules as shown in Figure 4a. The nanotube has a diameter of about 6.15 Å. The nanotube is periodic along the  $c$ -direction and is confined in the  $ab$ -plane. We used hexagonal super cells with in plane lattice parameter of about 16 Å, resulting in a vacuum of about 10 Å between the periodic images, thereby ensuring negligible interaction between them. Brillouin zone (BZ) integrations have been done with  $1 \times 1 \times 27$  Monkhorst-Pack k-point mesh. For the defects we have used a  $1 \times 1 \times 3$  supercell for

the nanotube. This results in about 3% defect concentration. For the nanotubes, we have performed spin polarized calculations. However, we do not observe any magnetic moments due to the presence of the defects.

## 4. RESULTS

**4.1. Crystal Structure of CdS Nanotubes from X-ray Diffraction Spectra.** Figures 2a and 2b show the X-ray diffraction (XRD) spectra of CdS nanotubes having different outer diameters and at different growth durations (length), respectively. The XRD pattern corresponding to nanotube with the smallest diameter (22 nm) is better resolved than those with the larger ones. Later in this section we show that this is due to the larger crystallite size of the nanotube with 22 nm diameter. The dominant XRD peak around  $2\theta$  value of  $26.7^\circ$  can either be indexed to (002) plane of hexagonally packed wurtzite phase of CdS (JCPDS 75-1545),<sup>38,39</sup> or to the (111) plane of CdS's cubic phase (zinc blende) (JCPDS 10-0454). The difference in the formation energies of these crystalline phases is very small.<sup>40–45</sup> Therefore, it is usually difficult to

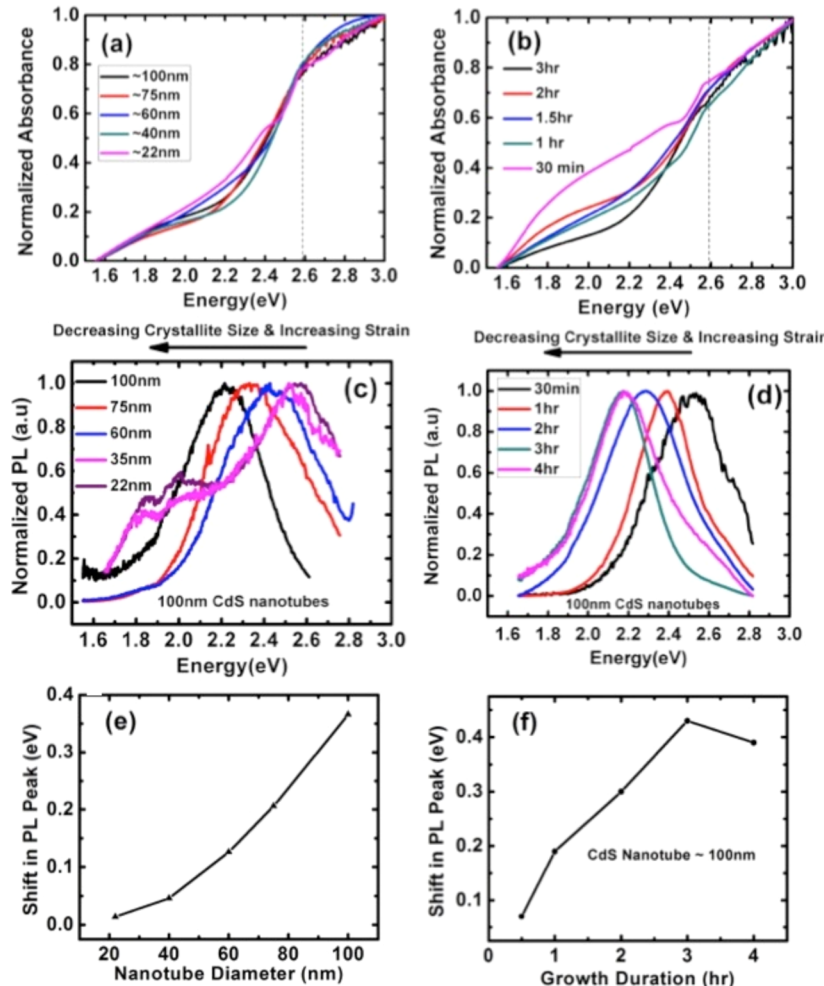


**Figure 3.** Absorbance spectra of CdS nanotubes as a function of their diameters (a) and growth durations (or lengths) for outer diameter of about 100 nm (b). PL spectra of the CdS nanotubes with increasing diameter (c) and growth duration/length (d). Quantitative estimates of these redshifts of PL peak from the absorbance edge of CdS nanotubes having different diameters and growth durations (or lengths) are plotted in (e) and (f), respectively.

identify the exact crystalline phase of these CdS nanotubes using powder XRD alone. However, for the wurtzite phase it is well-known that there can be additional peaks from the (100) and (101) planes (as shown in the same plots) that appear on both side of the peak from (002) plane, whereas these additional peaks around  $26.7^\circ$  are absent in the cubic phase. In Figures 2a and 2b, we see the presence of these additional XRD peaks in the form additional shoulders. These shoulders corresponding to these peaks are more prominent on both side of the dominant (002) peak at  $26.7^\circ$  for CdS nanotubes with smaller diameters. Therefore, we nominally assign the crystalline phase of these CdS nanotubes to hexagonally packed wurtzite structure. Moreover, it is also apparent that these CdS nanotubes possibly have a preferred growth direction along (002) plane as suggested by the overall dominance of the  $2\theta$  peak at  $26.7^\circ$ .

In the presence of such overlapping peaks and possible strain related broadening around  $26.7^\circ$ , it is difficult to determine the exact crystallite size using the Debye–Scherer method only. However, the Williamson–Hall method, which is generally used to extract information on purely strain related broadening, also requires a set of well-formed and nonoverlapping XRD peaks to differentiate it from size related broadening. In this work, we deconvoluted the dominant and composite XRD peak

around  $26.7^\circ$  with three Lorentzian line shapes and found the integral breadth ( $\beta = (\pi/2)\text{fwhm}$ , where fwhm represents the full width at half-maximum) corresponding to the central (002) peak for further use. The Debye–Scherer formula  $D = K\lambda/(\beta \cos \theta)$  then gives an estimate of crystalline size ( $D$ ) of all these CdS nanotubes for  $K = 0.9$  and  $\lambda = 0.154$  nm. From Figures 2c and 2d, we see that the crystallite sizes actually decreases with increasing outer diameter and length of these nanotubes, respectively. We roughly estimate the weighted average strain ( $\varepsilon$ ) in CdS nanotubes using  $\varepsilon = \beta/(4 \tan \theta)$ . Qualitative variations of these estimated strain are plotted in Figures 2e and 2f as a function of nanotube diameter and growth duration (length), respectively. Observed trends clearly reveal that crystalline strain progressively increases with increasing nanotube diameter and also with increasing nanotube length. Similar estimates based on other not-so-prominent XRD peaks also support the above systematic trend in crystallite size and crystalline strain (see Supporting Information). Therefore, we can fairly well assume that these CdS nanotubes with bigger overall dimensions (length and diameter) have smaller crystallite sizes with more structural strain. This information will be further used in our electronic structure calculations to explain the optical properties of these nanotubes.

**4.2. Optical Absorbance Spectra and the Shift in PL Spectrum of CdS Nanotubes Having Different Outer Diameters and Lengths.** Figures 3a and 3b show room temperature optical absorbance spectra of CdS nanotubes having different diameters and lengths, respectively. It is important to note that the absorbance edge/shoulder at approximately 2.6 eV does not vary significantly with changing outer diameter and length of these nanotubes. This is counterintuitive, as the absorbance edge was expected to blue-shift with decreasing crystallite sizes assuming that charge carriers are localized within the crystallite boundary (see Figure 2c,d). Furthermore, Figure 3c shows PL spectra of these CdS nanotubes having different diameters. These PL spectra were measured after photoexcitation at 2.95 eV which is above the absorbance edge of 2.6 eV. In sharp contrast to optical absorbance spectra, PL peak positions, however, systematically red-shift over a wide range of about 0.4 eV with increasing outer diameters (decreasing crystallite size), which cannot be anticipated from XRD results and the usual quantum confinement effects. It is rather common to expect that the smaller nanostructures with dimension comparable to the Bohr exciton radius (3 nm) of CdS should show a sizable blue-shift in both absorbance and PL spectra due to quantum confinement effects. However, it is also well-known that luminescence is always more susceptible to surface conditions than the absorbance spectra. While absorbance is primarily a reflection of the influence of quantum confinement on the joint density of state and the transition matrix element, luminescence requires radiative recombination of excited electron and holes, which can be strongly influenced by the presence of nonradiative surface defects at such small length scales. Depending on the nature of these surface defects, sub-band-gap trap levels are introduced by either cadmium or sulfur excess/vacancy in CdS nanotubes. This may eventually shift the emission peak either toward yellow or red side of the visible spectrum. PL from CdS nanotubes with smaller diameters (Figure 3c) does however display a strong emission band due to band edge emission around (2.57 and 2.51 eV) and other weak but even broader emission band of about 1.99 eV. Further, to understand the PL shift, we calculated the crystalline strain for CdS nanotubes and observed in Figure 2e,f that this crystalline strain is increasing with increasing size. Therefore, we tentatively ascribe such variation in PL spectrum not with quantum confinement effects but with the presence of crystalline strain and to strain induced variation of optically active surface defects at the surface of these CdS nanotubes. It will be interesting to figure out the density and the nature of these optically active surface defects which are acting as strong luminescence centers in these CdS nanotubes. Therefore, electronic structure calculations can provide us some interesting insights not only into the abundance of such luminescence centers but also into the nature of its influence on the PL spectrum as a function of the outer diameter of these nanotubes.

Moreover, CdS nanotubes with fixed outer diameter of 100 nm but having increasingly different lengths are prepared by increasing the growth duration of these nanotubes. Based on the SEM images, it was clearly established in the past<sup>26</sup> that the length of these nanotubes also increases with increasing the growth duration. Figure 3d shows that the PL spectra of these 100 nm wide CdS nanotubes grown for different durations. Like in Figure 3c, here also we see the distinct red-shift in PL peak position with increasing length of these CdS nanotubes, in

sharp contrast to its optical absorbance spectra (Figure 3b). PL measured for all CdS nanotubes having different lengths are also excited at 2.95 eV. Reported<sup>46,47</sup> electronic defects in CdS are mainly due to sulfur vacancy which lies around 0.7 eV from the conduction band and another defect from cadmium vacancy which lies 1.2 eV above valence band.<sup>48</sup> There are also reports of surface state defect level lying at about 0.2–0.4 eV below the conduction band,<sup>49,50</sup> which are responsible for band edge emission from CdS. Even if we take care of these known surface defects, it is very difficult to still identify and separate the contribution of each defect states toward the systematic red-shift in PL with increasing length of these CdS nanotubes without further theoretical understanding about their nature and role in light emission.

In Figures 3e and 3f, we plot the systematic red-shift of luminescence with respect to increasing nanotube diameter and increasing growth duration, respectively. As discussed above, this is quite the opposite if quantum confinement effects within smaller crystallite sizes are significant enough following Figures 2c and 2d. At this stage we want to emphasize that the estimated crystalline strain for different diameters and lengths of these CdS nanotubes (as seen in Figure 2e,f) seem to be increasing with the increase in overall size of these nanotubes. We had earlier established that the growth of these nanotubes actually nucleates at the nanotube interface with AAO. Therefore, we hypothesize that this in-built crystalline strain caused during the growth nucleation by structural bending of the nanotubes under their own weight may actually result in such systematic changes in the energy positions of defect states/luminescence centers on the CdS nanotube surface. We expect that further electronic structure calculations can identify such luminescence centers and also confirm this premise of strain induced shift of PL spectra.

### 4.3. Model System and First Principles Calculations.

To verify the above hypothesis and to understand the role of strain and to identify the nature of defects which affect the optical properties of these nanotubes, we performed first-principles density functional theory based calculations on a single shelled CdS nanotube, each unit cell containing six CdS molecules as shown in Figure 4. The nanotube is periodic along the *c*-direction and is confined in the *ab*-plane. Figure 4a shows the cross section of the bulk truncated nanotube before relaxation.

Structural relaxations of the nanotube result in significant changes of cell parameter *c*, the Cd–S bond lengths, and Cd–S–Cd bond angles as shown in Figure 4b,c. Compared to bulk CdS, the lattice parameter *c* of the nanotube reduces to 6.62 Å. The bulk truncated nanotube have a hexagonal cross section (Figure 4a). Upon relaxation, the surface undergoes significant relaxations and the cross section changes to that of a star-shaped one (Figure 4b). The Cd–S bond lengths ( $d_{\text{Cd-S}}$ ) shown in Figure 4c reduce to 2.50 Å compared to that of 2.56 Å in the bulk. The nanotube has a direct band gap (i.e., the valence band maxima (VBM) and the conduction band minima (CBM) are at the same k-point) of about 2.74 eV at  $\Gamma$ -point of the Brillouin zone (BZ), which is significantly higher than the DFT band gap of 1.12 eV for CdS bulk.

In order to explore whether it is thermodynamically possible to form these nanotubes, we have calculated the heat of formation and compared it with that of bulk CdS. The heat of formation ( $\Delta H^A$ ) of bulk CdS and the nanotube (A = bulk, nt) is given by

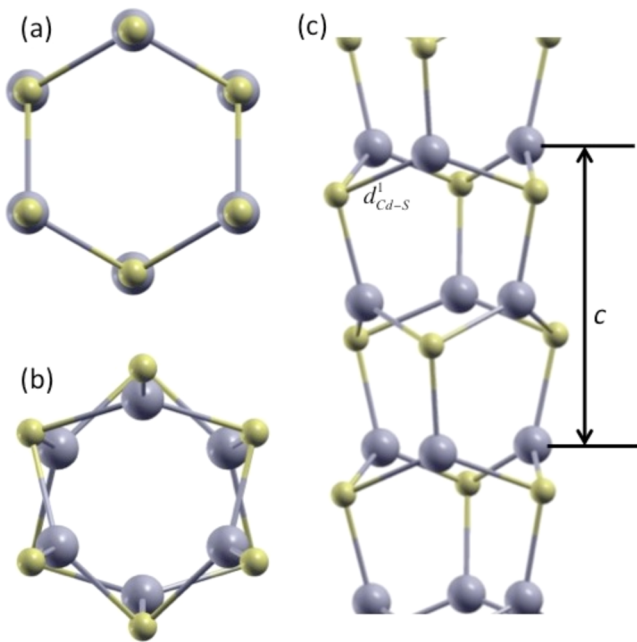


**Figure 4.** (a) Unrelaxed geometry of the CdS nanotube. The relaxed geometry of the CdS nanotube (b) top view and (c) side view.  $d_{\text{Cd}-\text{S}}^1$  denotes the Cd–S bond lengths, and  $c$  denotes the cell parameter. The S (Cd) atoms are denoted by yellow (gray) spheres.

$$\Delta H^A = \mu_A - \mu_{\text{Cd}}^0 - \mu_S^0 \quad (1)$$

where  $\mu_A$  is the chemical potential of CdS in bulk (when  $A = \text{bulk}$ ) or in the nanotube (when  $A = \text{nt}$ ). The chemical potentials for bulk CdS and the nanotube are obtained as the total energy of the primitive unit cell per formula unit. The elemental chemical potential  $\mu_Y^0$  ( $Y = \text{Cd}, \text{S}$ ) are given by total energy per atom of bulk Cd metal in the hcp structure and  $\text{S}_2$  molecule in gas phase in its spin triplet state. A negative value of the formation energy shows that it is possible to form the bulk or the CdS nanotube. For bulk CdS, we find  $\Delta H^{\text{bulk}} = -1.89$  eV, which is in excellent agreement with that obtained in ref 31. For the CdS nanotube, we find the formation energy to be  $-1.34$  eV. Though this is about  $0.55$  eV higher than that of bulk CdS, the negative sign indicates that it is thermodynamically possible to form these nanotubes.

As mentioned in the earlier part of this paper, the experimental results suggests that the nature of the defects and their concentration might play a crucial role in the photophysics of these nanotubes. The defect concentration depends exponentially on the defect formation energy ( $\Delta E^D(q)$ ) of a defect with charge  $q$ , which is given by

$$\Delta E^D(q) = E^D(q) - n_{\text{Cd}}\mu_{\text{Cd}} - n_S\mu_S + q(\mu_e + E_{\text{VBM}}) + \xi(q) \quad (2)$$

where  $E^D(q)$  is the total energy of the super cell with the charged defect and  $n_X$  and  $\mu_X$  are the number of atoms in the defective supercell and the atomic chemical potential of  $X$  ( $= \text{Cd}$  or  $\text{S}$ ), respectively.  $\mu_e$  is the electron chemical potential that determines the Fermi level and varies in the range of the band gap.  $E_{\text{VBM}}$  is the valence position of the valence band maximum of the defect-free system. The last term accounts for the electrostatic energy of point charges in an oppositely charged homogeneous medium (jellium background). Since we are

considering neutral defects, i.e.,  $q = 0$ , the above equation becomes

$$\Delta E^D = E^D - n_{\text{Cd}}\mu_{\text{Cd}} - n_S\mu_S \quad (3)$$

The equilibrium constraint on the atomic chemical potential is given by

$$\mu_A = \mu_{\text{Cd}} + \mu_S \quad (4)$$

Equation 3 together with eq 1 defines the range of the atomic chemical potential. In our experiments, the nanotubes grow on the  $\text{Na}_2\text{S}$  side of the reaction chamber, i.e., under S-rich conditions. Though the atomic chemical potentials depend on the experimental conditions (in our case, Cd and S are present in solutions as ions), it is possible to make use of the formation energies of Cd and S in its elemental states and the formation energies of the nanotubes to determine useful bounds in the chemical potentials. The thermodynamic stability of the nanotubes (given by negative formation energy as given in the earlier part of this section) implies that the chemical potentials of Cd and S cannot be higher in the nanotubes than in their elemental states,  $\text{S}_2$  molecule in gas phase in spin triplet state, and bulk metallic Cd in hcp structure. Hence,  $\mu_{\text{Cd}} \leq \mu_{\text{Cd}}^0$  and  $\mu_S \leq \mu_S^0$ . The S-rich growth condition can be achieved by putting  $\mu_S = \mu_S^0$  in eq 3. The corresponding value for  $\mu_{\text{Cd}}$  is obtained from eqs 1 and 4. Using these two equations, we get  $\mu_{\text{Cd}} = \mu_{\text{Cd}}^0 + \Delta H^A$ .

Among the different possible defects, we have considered four types of isolated native stoichiometric defects in the nanotube: (i) a Cd vacancy ( $V_{\text{Cd}}^{\text{nt}}$ ), (ii) a S vacancy ( $V_S^{\text{nt}}$ ), (iii) a Cd interstitial ( $\text{Cd}_i^{\text{nt}}$ ), and (iv) a S interstitial ( $S_i^{\text{nt}}$ ) in their neutral charge state. For each type of defect we also optimized the lattice parameter. In all these cases there is a slight increase in the lattice parameter compared to that of the defect-free nanotube. To compare the defect formation energies in the nanotube with those in the bulk, we have also considered isolated Cd vacancy ( $V_{\text{Cd}}^b$ ) and S vacancy ( $V_S^b$ ) in  $3 \times 3 \times 2$  bulk CdS unit cells. Since the experiments were done in S-rich conditions (the nanotubes grow on the  $\text{Na}_2\text{S}$  side), we have calculated the defect formation energies in the S-rich condition, and their values are listed in Table 1. In contrast to that of the bulk, the  $\Delta E^D$  of similar defects in the nanotube are much lower, indicating that the nanotubes are more prone to defects compared to that of the bulk.

When a Cd atom is removed to create a Cd vacancy ( $V_{\text{Cd}}^{\text{nt}}$ ), there are three dangling bonds on the S atoms which were bound with the Cd atom. Upon geometry optimization, the local geometry of the nanotube around the defect changes significantly. Of the three S atoms, two of them move closer and form a dimer with S–S bond length of  $2.12$  Å (Figure 5a).

**Table 1. Defect Formation Energies of Different Defects in S-Rich Condition<sup>a</sup>**

system	defect type	defect formation energy ( $\Delta E^D$ ) S-rich (eV)
bulk	$V_{\text{Cd}}^b$	2.26
	$V_S^b$	3.34
nanotube	$V_{\text{Cd}}^{\text{nt}}$	0.90
	$V_S^{\text{nt}}$	2.19
	$\text{Cd}_i^{\text{nt}}$	1.79
	$S_i^{\text{nt}}$	0.24

<sup>a</sup>The notations used to denote the defect types are described in the text.

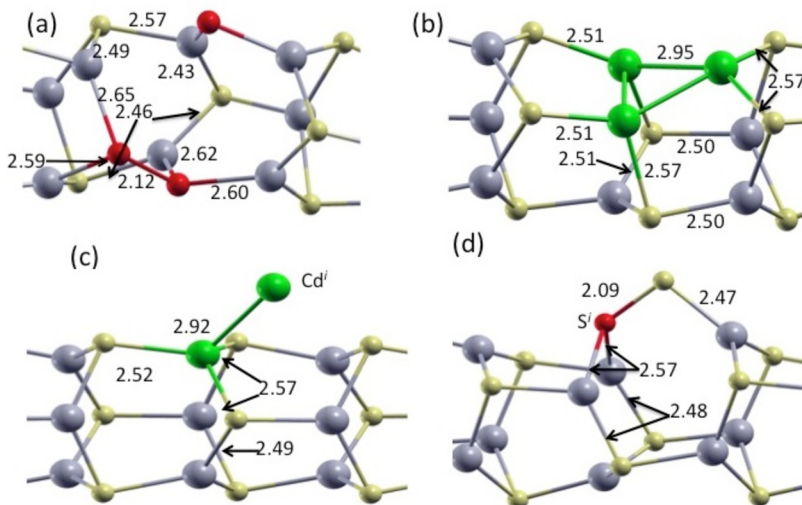


**Figure 5.** (a) Relaxed geometry and relevant bond lengths of the CdS nanotube with Cd vacancy (a), S vacancy (b), Cd interstitial (c), and S interstitial (d). The bond lengths are given in Å. The S (Cd) atoms involved in the defect are shown in red (green) spheres. The other S (Cd) atoms are denoted by yellow (gray) spheres.

However, the S–S bond length is much longer than that of an isolated  $S_2$  (1.89 Å) molecule. In case of the isolated sulfur molecule, the  $p\pi\pi^*$  state is occupied by two electrons with parallel spin giving rise to the triplet ground state. However, in this case, the S atoms in the dimer interact with the four neighboring Cd atoms. These Cd atoms donate two electrons to the  $p\pi\pi^*$  state of  $S_2$  resulting in a  $s-p\pi\pi^*$  state below the VBM. This also explains the increase in the S–S bond length. Simultaneously, we find an unoccupied electronic state about 0.15 eV below the CBM of the pristine nanotube (Figure 6)

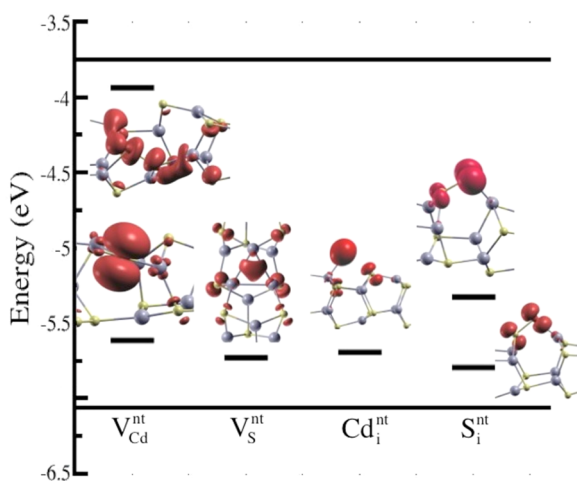


**Figure 6.** Relative position of the defect levels (and their localization of the corresponding wave function in real space) with respect to valence band and conduction band of the defect-free nanotube.

arising from the hybridization of the Cd-s and the  $p\pi\pi^*$  of the “molecular” S (Cd-mol-S). Similar diatomic molecular form of O atoms associated with O interstitials have been reported by Janotti et al. in bulk ZnO.<sup>51</sup> We note that similar rearrangement of the atoms are not observed when a Cd vacancy is formed in bulk CdS. The neighboring Cd–S bond lengths have increased by about 4–6% compared to that of the defect-free nanotube. The third dangling bond on the S atom which is partially occupied forms an acceptor state at about 0.46 eV above the

VBM (Figure 6). Though this defect has the second lowest formation energy (0.90 eV), however, as we will show later, it plays a crucial role in the optical properties of the CdS nanotube.

Among the native defects, the sulfur vacancy ( $V_S^{nt}$ ) acts as donor. However, in a S-rich environment, it has the largest formation energy of 2.19 eV, and it is highly unlikely that these will form. Upon relaxation, the three Cd atoms which were bound to the S atom (that has been removed to form the S vacancy) form a trimer with a Cd–Cd bond length of 2.95 Å. This is similar to the bulk Cd–Cd bond length of 2.97 Å in bulk hcp-Cd. The Cd–S bond lengths around the vacancy remains almost same as that found in the pristine nanotube as shown in Figure 5b. Similar to O vacancies in bulk ZnO, S vacancies in the CdS nanotube also form a deep donor state at about 0.33 eV above the VBM (Figure 6).

For Cd interstitial ( $Cd_i^{nt}$ ), we tried different possible configurations in which the Cd atom was put inside the nanotube and also at the surface. For both the cases, the Cd atoms move away from the nanotube and attains the structure shown in Figure 5c. The Cd–Cd<sub>i</sub> bond length in this case is 2.92 Å, and the Cd<sub>i</sub>–S bond length is 3.16 Å. The formation energy of this defect is also quite high (1.79 eV) in S-rich condition and is unlikely to form. The Cd<sub>i</sub><sup>nt</sup> introduces a defect state filled with two electrons at about 0.37 eV above the VBM (Figure 6).

Like the Cd interstitials, the S interstitial ( $S_i^{nt}$ ) can also occupy more than one possible site. Either it can be inside the tube or it can be on the surface. Starting from the above two configuration, upon relaxation, the S interstitial forms a geometry as shown in Figure 5d. This defect has the lowest formation energy (0.24 eV). Analogous to that of O interstitials in bulk ZnO, the S interstitial relaxes to a split interstitial where it shares a lattice site with the nearest-neighbor S atom. Similar to the dimer formed in case of the Cd vacancy, in this case the S atoms forms molecular S with an elongated bond length of 2.09 Å. The elongation of the S–S bond length is due to the filling up of the half filled  $p\pi\pi^*$  state (in case of isolated molecule) by electrons received from the neighboring Cd ions. However, unlike the S–S bond in case of Cd vacancy, here the

degeneracy between the two states is broken because the two S atoms of the dimer interact differently with the Cd atoms. While S atom from the lattice binds to two Cd atoms, the interstitial S atom ( $S_i$ ) binds to just a single Cd atom. These two states are seen at 0.26 and 0.78 eV above the VBM of the pristine nanotube (Figure 6). Moreover, both these states are completely occupied and will not play an active role in the optical properties of these nanotubes.

The results from the calculations can be summarized as follows: (a) In the nanotubes, the S interstitials will be most abundant, followed by Cd vacancies; the formation energies of the other two defects are so high that it is unlikely that they will be formed. (b) The defect states arising from the S interstitial are completely occupied while those due to the Cd vacancy are either partially occupied or completely empty. These indicate that while the S interstitials may be in abundance in the nanotubes, these are optically inactive, and it is the partially occupied/empty states arising from the defects in the form of Cd vacancies, which are actually the minority in terms of their concentration as compared to the S interstitials, might play a crucial role in the PL properties of these nanotubes.

The experimental results presented in Figure 2b,c show that as the size (diameter or length) of the nanotubes increases, they are subject to tensile strain. We note that this strain may not be homogeneous but rather local around the defects due to the change in the bond lengths as the system relaxes to its ground state once the defect is formed. This strain not only might affect the positions of the VBM and CBM of the nanotubes but also might result in shift of the positions of the defect states in the gap. Hence, to get a complete understanding, we have also studied the effects of strain on the position of the VBM and CBM of the pristine nanotube and the defect states. However, to model the inhomogeneous strain in the system, an enormously large supercell is necessary, which would increase the computational cost. Hence, to understand the effect of strain on the position of the conduction and valence bands of the pristine nanotube and on the position of the defect states arising from isolated defects, we have limited ourselves to the case of homogeneous strain. We have invoked effect of strain in our calculations by varying their  $c$  from -4% to 5% of that of the  $c$  of the pristine nanotube. This results to subjecting the nanotubes to axial strain (both compressive and tensile). The results are presented in Figure 7. For the defect-free nanotube we find that the position of the VBM and CBM does not show any significant change as it is compressed or expanded. Similarly for the nanotubes with S vacancy, Cd interstitial, and S interstitial, a slight shift is seen in the position of the defect states as a function of strain. However, for the Cd vacancy (this has the second lowest defect formation energy), the acceptor defect state above the VBM and the Cd-mol-S state below the CBM move closer to each other as the nanotube is elongated, thereby reducing the effective gap of the system.

## 5. DISCUSSION AND SUMMARY

As the length/diameter of the nanotubes increase, the crystalline strain in them also increases. However, the measured absorption spectra of the CdS nanotubes do not show any shift in the band gap, neither as a function of their length nor as a function of their diameter (Figure 3a,b), suggesting that the electronic states involved during the optical absorption process is not influenced by strain. From our calculations we find that the positions of the occupied VBM, the unoccupied CBM, and

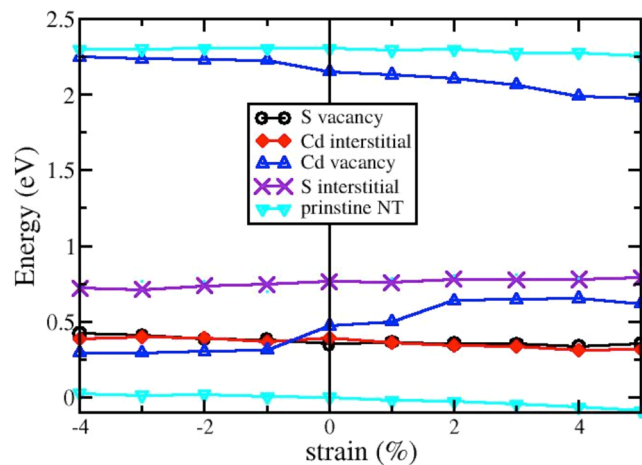


**Figure 7.** Variation of the VBM and CBM of the pristine nanotube and the shift in the position of the defect states with strain. The VBM of the pristine unstrained nanotube is set to zero, and all the other states are aligned with respect to it.

the occupied defect states from the S interstitials of the model CdS nanotube are almost unaffected by strain. Therefore, we can conclude that the electrons which are excited during optical absorption process are from the above-mentioned occupied states. However, the probability of transition involving the states arising from the S interstitial and the conduction band of the nanotubes are low because (a) the density of these defect states are very low and (b) while the CBM is at  $\Gamma$ -point of the BZ, these states are at the A-point of the one-dimensional BZ, resulting in a very weak coupling between these states. Hence, in the absorption spectra measurements, only the VB and the CB of the nanotubes are involved.

Unlike the absorption spectra, the PL spectra shows that there is a red-shift of the emission peak as the nanotubes grow. Similar shifts are also observed in case of ZnO<sup>14</sup> and CdSe<sup>15</sup> nanotubes. Our calculations suggest that only the states arising from the Cd vacancies will act as luminescent centers. This is because the states due to the abundantly present S interstitials (these defects have the highest concentration) are completely occupied and hence cannot take part in the PL process, and the other defects are unlikely to be formed due to their very high formation energies. During the PL measurement the electrons from the valence band are excited to the high energy states in the conduction band (in the PL experiments the electrons are excited at 2.95 eV which is much larger than the band gap). These electrons then decay down to the empty Cd-mol-S state, arising from the Cd vacancy, just below the CBM. On reaching the Cd-mol-S state, the electron recombines with a hole present in the partially filled acceptor state arising from the Cd vacancy, giving rise to the emission maxima. The position of the emission peak gives the effective band gap ( $E_g$ ) of the system. Our calculations predict the  $E_g$  to be 1.68 eV, which is underestimated by about 0.87 eV compared to the emission maxima for the shortest nanotube. However, this is typical of DFT calculations. To get more accurate estimates of the band gap, one needs to use hybrid functionals or perform more accurate GW calculations. However, both are computationally very expensive and are beyond the scope of the present study.

During the growth, the nucleation sites at the interface of AAO and CdS nanotube experience tensile strain because of the increase in the weight of the nanotubes. This way crystalline strain is incorporated in the nanotube structure. As mentioned

earlier, from our calculations we find that only Cd vacancies (which have the second highest defect concentration) are significantly affected by the strain. The tensile strain reduces the  $E_g$  from 1.68 eV (at 0% strain) to 1.35 eV (at 5% strain), resulting in the red-shift of the emission spectra as the overall size of the nanotube is increased. Our calculations predict a red-shift of 0.33 eV, which is in reasonably good agreement with that measured in the experiment (about 0.4 eV). The red-shift of the nanotubes as a function of the diameter can also be explained with similar arguments. As the radius of the nanotubes increase, the surface experiences a tensile strain. The defect states shift in a similar manner under the strain, resulting in the red-shift of the PL spectra.

In summary, we have investigated the optical properties of the nicely ordered array of CdS nanotubes synthesized by an unique nanofabrication technique in a S-rich environment. The absorption spectra of the nanotubes as a function of their length and diameter do not show any significant shift in the absorption peak because the transition giving rise to the absorbance peak involves the valence and conduction bands which do not change significantly with strain. However, interestingly, the PL spectra shows a red-shift in the emission peak as the length or diameter of the nanotubes increases. From our calculations on a model system we attribute this shift in the emission peak of the PL spectra to an interplay between the strain experienced by the nanotubes with the increase in size and Cd vacancies formed during the synthesis or growth of the nanotubes. The experimental observations in combination with the calculations show that in the PL the minority defect Cd vacancies are involved, and their positions change with strain. We note that though these defects may not be abundant in the nanotubes (they have the second lowest value of formation energies), these are crucial in determining the optical properties of the nanotubes. Usually it is expected that the defect with *largest* concentration plays the most important role in the optical properties of these nanotubes. However, the experiments and the calculations reported in this paper suggests that rather than the *concentration*, it is the *nature* of the defect which is crucial.

## ASSOCIATED CONTENT

### Supporting Information

Plots showing the calculated crystallite size or strain from other peaks in the XRD spectra. This material is available free of charge via the Internet at <http://pubs.acs.org>.

## AUTHOR INFORMATION

### Corresponding Authors

\*E-mail: pghosh@iiserpune.ac.in (P.G.).

\*E-mail: shouvik@iiserpune.ac.in (S.D.).

### Notes

The authors declare no competing financial interest.

## ACKNOWLEDGMENTS

The authors thank IISER-Pune for startup funding of the laboratory infrastructure as well as the grant no. SR/S2/CMP-72/2012 and DST Nano Unit grant SR/NM/NS-42/2009 from Dept. of Science and Technology, India. The authors acknowledge Dr. Angshuman Nag, IISER Pune, and Dr. Tiju Thomas, IISc. Bangalore, India, for useful discussions. P.G. acknowledges Centre for Development of Advanced Computing, Pune, India, for providing computing facility and DST-

Nano Mission, Project No. SR/NM/NS-15/2011 for financial support.

## REFERENCES

- (1) Scholes, G. D.; Rumbles, G. Excitons in Nanoscale Systems. *Nat. Mater.* **2006**, *5*, 683–696.
- (2) Kelly, K. L.; Coronado, E.; Zhao, L. L.; Schatz, G. C. The Optical Properties of Metal Nanoparticles: the Influence of Size, Shape, and Dielectric environment. *J. Phys. Chem. B* **2003**, *107*, 668–677.
- (3) Trindade, T.; O'Brien, P.; Pickett, N. L. Nanocrystalline Semiconductors: Synthesis, Properties, and Perspectives. *Chem. Mater.* **2001**, *13*, 3843–3858.
- (4) Wang, X.; Wang, Z. M.; Liang, B.; Salamo, G. J.; Shih, C. K. Direct Spectroscopic Evidence For the Formation of One-dimensional Wetting Wires during the Growth of InGaAs/GaAs Quantum Dot Chains. *Nano Lett.* **2006**, *6*, 1847–1851.
- (5) Fan, Z.; Razavi, H.; Do, J.; Moriawaki, A.; Ergen, O.; Chueh, Y. L.; Leu, P. W.; Ho, J. C.; Takahashi, T.; Reichertz, L. A. Three-Dimensional Nanopillar-Array Photovoltaics on Low-Cost and Flexible Substrates. *Nat. Mater.* **2009**, *8*, 648–653.
- (6) Duan, X.; Huang, Y.; Agarwal, R.; Lieber, C. M. Single-Nanowire Electrically Driven Lasers. *Nature* **2003**, *421*, 241–245.
- (7) Ma, R. M.; Dai, L.; Huo, H. B.; Xu, W. J.; Qin, G. G. High-Performance Logic Circuits Constructed on Single CdS Nanowires. *Nano Lett.* **2007**, *7*, 3300–3304.
- (8) Li, L.; Wu, P.; Fang, X.; Zhai, T.; Dai, L.; Liao, M.; Koide, Y.; Wang, H.; Bando, Y.; Golberg, D. Single-Crystalline CdS Nanobelts for Excellent Field-Emitters and Ultrahigh Quantum-Efficiency Photodetectors. *Adv. Mater.* **2010**, *22*, 3161–3165.
- (9) Kim, J. I.; Kim, J.; Lee, J.; Jung, D.-R.; Kim, H.; Choi, H.; Lee, S.; Byun, S.; Kang, S.; Park, B. Photoluminescence Enhancement in CdS Quantum Dots by Thermal Annealing. *Nanoscale Res. Lett.* **2012**, *7*, 482.
- (10) Wuister, S. F.; Driel, F. V.; Meijerink, A. Luminescence and Growth of CdTe Quantum Dots and Clusters. *Phys. Chem. Chem. Phys.* **2003**, *5*, 1253.
- (11) Zheng, J.; Huang, F.; Yin, S.; Wang, Y.; Lin, Z.; Wu, X.; Zhao, Y. Correlation Between the Photoluminescence and Oriented Attachment Growth Mechanism of CdS Quantum Dots. *J. Am. Chem. Soc.* **2010**, *132*, 9528–9530.
- (12) Sun, L.; Kim, D. H.; Oh, K. H.; Agarwal, R. Strain-Induced Large Exciton Energy Shifts in Buckled CdS Nanowires. *Nano Lett.* **2013**, *13*, 3836–3842.
- (13) Han, X.; Kou, L.; Zhang, Z.; Zhu, X.; Xu, J.; Liao, Z.; Guo, W.; Yu, D. Strain-Gradient Effect on Energy Bands in Bent ZnO Microwires. *Adv. Mater.* **2012**, *24*, 4707–4711.
- (14) Chen, C.-W.; Chen, K.-H.; Shen, C.-H.; Ganguly, A.; Chen, L.-C.; Wu, J.-J.; Pong, W.-F. Anomalous Blue-Shift in Emission Spectra of ZnO Nanorods with Sizes Beyond Quantum Confinement Regime. *Appl. Phys. Lett.* **2006**, *88*, 241905.
- (15) Yan, Y.; Liao, Z.-M.; Bie, Y.-Q.; Wu, H.-C.; Zhou, Y.-B.; Fu, X.-W.; Yu, D.-P. Luminescence Blue-Shift of CdSe Nano Wires Beyond the Quantum Confinement Regime. *Appl. Phys. Lett.* **2011**, *99*, 103103.
- (16) Oulton, R. F.; Sorger, V. J.; Zentgraf, T.; Ma, R. M.; Gladden, C.; Dai, L.; Bartal, G.; Zhang, X. Plasmon Lasers at Deep Subwavelength Scale. *Nature* **2009**, *461*, 629–632.
- (17) Zhai, T. Y.; Fang, X. S.; Li, L.; Bando, Y.; Golberg, D. One-Dimensional CdS Nanostructures: Synthesis, Properties, and Applications. *Nanoscale* **2010**, *2*, 168–187.
- (18) Shen, X. P.; Yuan, A. H.; Wang, F.; Hong, J. M.; Xu, Z. Fabrication of Well-Aligned CdS Nanotubes by CVD-Template Method. *Solid State Commun.* **2005**, *133*, 19–22.
- (19) Shay, J. L.; Wagner, S.; Kasper, H. M. Efficient CuInSe<sub>2</sub>/CdS Solar Cells. *Appl. Phys. Lett.* **1975**, *27*, 89–90.
- (20) Dobson, K. D.; Visoly-Fischer, I.; Hodes, G.; Cahen, D. Stability of CdTe/CdS Thin-Film Solar Cells. *Sol. Energy Mater. Sol. Cells* **2000**, *62*, 295–325.

- (21) Matsumura, M.; Furukawa, S.; Saho, Y.; Tsubomura, H. Cadmium Sulfide Photocatalyzed Hydrogen Production from Aqueous Solutions of Sulfite: Effect of Crystal Structure and Preparation Method of the Catalyst. *J. Phys. Chem.* **1985**, *89*, 1327–1329.
- (22) Jang, J. S.; Joshi, U. A.; Lee, J. S. Solvothermal Synthesis of CdS Nanowires for Photocatalytic Hydrogen and Electricity Production. *J. Phys. Chem. C* **2007**, *111*, 13280–13287.
- (23) Bao, N. Z.; Shen, L. M.; Takata, T.; Domen, K. Self-Templated Synthesis of Nanoporous CdS Nanostructures for Highly Efficient Photocatalytic Hydrogen Production under Visible Light. *Chem. Mater.* **2008**, *20*, 110–117.
- (24) Xu, X.; Zhao, Y.; Sie, E. J.; Lu, Y.; Liu, B.; Ekahana, S. A.; Ju, X.; Jiang, Q.; Wang, J.; Sun, H.; et al. Dynamics of Bound Exciton Complexes in CdS Nanobelts. *ACS Nano* **2011**, *5*, 3660–3669.
- (25) Xiong, Q.; Chen, G.; Acord, J. D.; Liu, X.; Zengel, J. J.; Gutierrez, H. R.; Redwing, J. M.; Voon, L. C. L. Y.; Lassen, B.; Eklund, P. C. Optical Properties of Rectangular Cross-Sectional ZnS Nanowires. *Nano Lett.* **2004**, *4*, 1663–1668.
- (26) Varghese, A.; Datta, S. Directionally Asymmetric Self-assembly of Cadmium Sulfide Nanotubes Using Porous Alumina Nanoreactors: Need for Chemohydrodynamic Instability at the Nanoscale. *Phys. Rev. E* **2012**, *85*, 056104.
- (27) Giannozzi, P.; Baroni, S.; Bonini, N.; Calandra, M.; Car, R.; Cavazzoni, C.; Ceresoli, D.; Chiarotti, G. L.; Cococcioni, M.; Dabo, I.; et al. R. M. QUANTUM ESPRESSO: a Modular and Open-Source Software Project for Quantum Simulations of Materials. *J. Phys.: Condens. Matter* **2009**, *21*, 395502.
- (28) Perdew, J.; Burke, K.; Ernzerhof, M. Generalized Gradient Approximation Made Simple. *Phys. Rev. Lett.* **1996**, *77*, 3865–3868.
- (29) Vanderbilt, D. Soft Self-Consistent Pseudopotentials in a Generalized Eigenvalue Formalism. *Phys. Rev. B* **1990**, *41*, 7892–7895.
- (30) Marzari, N.; Vanderbilt, D. Thermal Contraction and Disordering of the Al(110) Surface. *Phys. Rev. Lett.* **1999**, *82*, 3296–3299.
- (31) Nishidate, K.; Sato, T.; Matsukura, Y.; Baba, M.; Hasegawa, M.; Sasaki, T. Density-Functional Electronic Structure Calculations for Native Defects and Cu Impurities in CdS. *Phys. Rev. B* **2006**, *74*, 035210.
- (32) Razik, N. A. Use of a Standard Reference Material for Precise Lattice Parameter Determination of Materials of Hexagonal Crystal Structure. *J. Mater. Sci. Lett.* **1987**, *6*, 1443–1444.
- (33) Camacho, J.; Cantarero, A. Lattice Dynamics in Wurtzite Semiconductors: The Bond Charge Model of CdS. *Phys. Status Solidi B* **1999**, *215*, 181–187.
- (34) CRC Handbook of Chemistry and Physics, 82nd ed.; CRC Press: New York, 2001.
- (35) Huang, M. H.; Mao, S.; Feick, H.; Yan, H.; Wu, Y.; Kind, H.; Weber, E.; Russo, R.; Yang, P. Room-Temperature Ultraviolet Nanowire Nanolasers. *Science* **2001**, *292*, 1897–1899.
- (36) Wang, J.; Gudiksen, M. S.; Duan, X.; Cui, Y.; Lieber, C. M. Highly Polarized Photoluminescence and Photodetection From Single Indium Phosphide Nanowires. *Science* **2001**, *293*, 1455–1457.
- (37) Zhu, Y.-P.; Li, J.; Ma, T.-Y.; Liu, Y.-P.; Du, G.; Yuan, Z.-Y. Sonochemistry-Assisted Synthesis and Optical Properties of Mesoporous ZnS Nanomaterials. *J. Mater. Chem. A* **2014**, *2*, 1093–1101.
- (38) Fan, D.; Thomas, P. J.; O'Brien, P. Deposition of CdS and ZnS Thin Films at the Water/Toluene Interface. *J. Mater. Chem.* **2007**, *17*, 1381–1386.
- (39) Li, X.; Chu, H.; Li, Y. Sacrificial Template Growth of CdS Nanotubes From Cd(OH)<sub>2</sub> Nanowires. *J. Solid State Chem.* **2006**, *179*, 96–102.
- (40) Bandaranayake, R. J.; Wen, G. W.; Lin, J. Y.; Jiang, H. X.; Sorensen, C. M. Structural Phase Behavior in II-VI Semiconductor Nanoparticles. *Appl. Phys. Lett.* **1995**, *67*, 831.
- (41) Ghosh, A.; Paul, S.; Raj, S. Structural Phase Transformation from Wurtzite to Zinc-Blende in Uncapped CdS Nanoparticles. *Solid State Commun.* **2013**, *154*, 25–29.
- (42) Ricolleau, C.; Audinet, L.; Gandais, M.; Gacoin, T. Structural Transformations in II-VI Semiconductor Nanocrystals. *Eur. Phys. J. D* **1999**, *9*, 565–570.
- (43) Soni, U.; Arora, V.; Sapra, S. Wurtzite or Zinc Blende? Surface Decides the Crystal Structure of Nanocrystals. *CrystEngComm* **2013**, *15*, 5458–5463.
- (44) Banerjee, R.; Jayakrishnan, R.; Ayyub, P. Effect of the Size-Induced Structural Transformation On the Band Gap in CdS Nanoparticles. *J. Phys.: Condens. Matter* **2000**, *12*, 10647–10654.
- (45) Xiong, Y.; Zhang, J.; Huang, F.; Ren, G.; Liu, W.; Li, D.; Wang, C.; Lin, Z. Phase-Transformation Mechanisms of Nanocrystalline CdS in Na<sub>2</sub>S Solution. *J. Phys. Chem. C* **2008**, *112*, 9229–9233.
- (46) Liu, B.; Xu, G. Q.; Gan, L. M.; Chew, C. H.; Li, W. S.; Shen, Z. X. Photoluminescence and Structural Characteristics of CdS Nano-clusters Synthesized by Hydrothermal Microemulsion. *J. Appl. Phys.* **2001**, *89*, 1059–1063.
- (47) Varghese, A. Enhanced Photoluminescence from Ordered Arrays of Cadmium Sulfide Nanotubes Synthesized Using Nanoscale Chemical Reactors. *J. Nanosci. Nanotechnol.* **2014**, *14*, 4495–4499.
- (48) Vigil, O.; Riech, I.; Garcia-Rocha, M.; Zelaya-Angel, O. Characterization of Defect Levels in Chemically Deposited CdS Films in the Cubic-to-Hexagonal Phase Transition. *J. Vac. Sci. Technol., A* **1997**, *15*, 2282.
- (49) Levine, J. D.; Mark, P. Theory and Observation of Intrinsic Surface States on Ionic Crystal. *Phys. Rev. E* **1966**, *144*, 751–763.
- (50) Xiong, S.; Xi, B.; Wang, C.; Zou, G.; Fei, L.; Wang, W.; Qian, Y. Shape-Controlled Synthesis of 3D and 1D Structures of CdS in a Binary Solution with L-Cysteine's Assistance. *Chem.—Eur. J.* **2007**, *13*, 3076–3081.
- (51) Janotti, A.; Van de Walle, C. G. Native Point Defects in ZnO. *Phys. Rev. B* **2007**, *76*, 165202.